European Journal of Physics

PAPER

Observing the polarization of cosmic-ray muons in student physics laboratory

To cite this article: Jisi Xu *et al* 2021 *Eur. J. Phys.* **42** 035603

IOP Publishing European Journal of Physics
Eur. J. Phys. **42** (2021) 035603 (13pp) https://doi.org/10.1088/1361-6404/abd87f

Observing the polarization of cosmic-ray muons in student physics laboratory

Jisi Xu, Anjun Chu, Zi Yuan, Xinliang Song, Tianle Cheng, Han Yi, Yijie Wang, Ying Chang, Zhao Zhang and Zhigang Xiao*

Department of Physics, Tsinghua University, Beijing 100084, People's Republic of China

E-mail: xiaozg@tsinghua.edu.cn

Received 14 October 2020, revised 16 December 2020
Accepted for publication 5 January 2021
Published 1 March 2021

Abstract

An undergraduate-level student experiment has been designed and implemented to measure the forward–backward asymmetry of the decay of the cosmic-ray muons, offering a pedagogical view to the parity violation in weak interactions. The detector system consists of six plastic scintillators installed vertically in row. The backward–forward asymmetry of the decay e^- and e^+ with respect to the muon motion direction is correlated with the incident depth of the muon stopped in the scintillator. MC simulations have been carried out in order to better interpret the data and optimize the data analysis. The forward–backward asymmetry of 0.051 ± 0.027 is deduced for the decay of cosmic-ray muons in the energy range being studied. The results are consistent with the picture of parity violation in weak interactions. The experiment can be constructed by the senior undergraduate students under the guidance of the course teacher.

Keywords: student experiment, cosmic-ray muon, polarization

(Some figures may appear in colour only in the online journal)

1. Introduction

Parity violation (PV) in weak interaction, one of the fundamental interactions in nature, was first suggested by Lee and Yang in 1950s [1]. Experimental confirmation was soon achieved in β decay of ^{60}Co nuclei [2, 3], in the electron capture of ^{152}Eu nuclei [4] and in the meson–muon–electron weak decay chain in accelerator-based experiments [5]. Since the discovery of PV in weak interaction is an extremely important and fundamental milestone in the development of modern physics, it is of great scientific interest to show this effect in a semi-quantitative way in the physics laboratory for undergraduate students.

*Author to whom any corresponence should be addressed.

In quantum field theory it is well understood that PV originates from the V–A structure of the weak interaction vertex, for which the introduction of the helicity projection operator $(1-\gamma^5)/2$ leads to the spin structure of weak interaction. As a result, only left-handed fermions or right-handed anti-fermions are coupled to interaction vertex in relativistic limit [6]. The PV effect manifests itself in the forward–backward asymmetry of the electrons in the β decay of nuclei with non-zero spin like ^{60}Co and in the polarization of the muons produced in the two-body weak decay of meson, for instance, $\pi^{\pm} \rightarrow \mu^{\pm} + \nu_{\mu}$, where ν_{μ} denotes the associated neutrino or anti-neutrino.

The polarized muons, originated mainly from two sources including the decay of meson beam produced by modern accelerator and by the high-energy cosmic-ray primaries, find many exciting applications in various scientific fields, ranging from the μ spin spectroscopy [7], μ spin rotation radiography [8, 9] to the proton radius measurement via μ-atom [10] as well as particle physics. Particularly, the charged cosmic-ray detected in terrestrial laboratory at sea level are dominated by the muons from the decay of mesons (approximately 90% of π) produced by the interactions of high-energy cosmic-ray primaries with atmospheric nuclei at high altitudes. In order to demonstrate the modern instrumentation and method in particle physics and application fields without building complex accelerator, many interesting educational experiments in student laboratory making use of cosmic-ray muons have been built or proposed [11, 12].

Our motivation is to build a student laboratory experiment aiming at the demonstration of PV in particle physics by making use of the cosmic-ray muons. In this paper, we describe an experiment designed for senior undergraduate students in physics laboratory. Special attention is paid on the pattern showing that up–down asymmetry varies with the depth of the stopped muon in the detector material. A non-zero up–down asymmetry is deduced. Section 2 describes the experimental method and the setup. Section 3 presents the simulation results and the data processing method. Section 4 presents the data analysis and the experimental results. Section 5 is the summary.

2. Experimental method and apparatus

The non-zero polarization of the cosmic-ray muons detected at sea level can be regarded as a relic of PV in weak interactions based on the following reasons. In the rest frame of the π meson, which is of spin zero, the decay muons are completely polarized in the direction of the motion of the former because the associate relativistic neutrino (anti-neutrino) is purely left-handed (right-handed). Specifically, the polarization is positive (negative) for negative (positive) muons. The degree of polarization of the muons in laboratory reference frame is partly maintained depending on the velocity and original direction of the muons with respect to the motion of the mother meson. Taking the μ^+ flux hitting down on the detector from high space for instance, we considered three extreme scenarios which can be detected on ground, as shown in figures 1(a)–(c), respectively. (i) The meson flies down and the μ^+ emitted in the direction of meson's motion, the polarization of μ^+ keeps negative with the momentum higher than the mother meson, (ii) the meson flies down while the μ^+ emitted opposite to the motion of the meson, the polarization is flipped to positive in laboratory and the momentum of the meson shall be much higher than that of the muon, and (iii) the meson flies upwards while the muon is emitted in the opposite direction, the polarization keeps negative and the momentum of the meson is much smaller than the detected muon. Thus, if the energy spectrum of the positively charged meson is such that the intensity falls off with energy, in a certain energy window of the detected muons, net negative polarization of μ^+ will be observed. Given that the μ^+ is less depolarized when it slows down and is stopped in material in comparison with μ^- due to

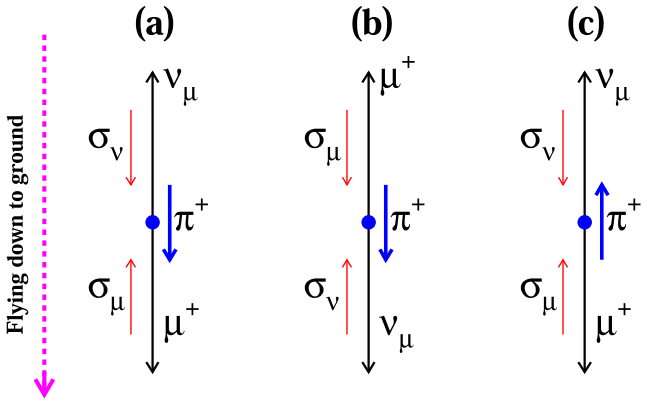

Figure 1. The schematic view of the decay of π^+ in three kinetic scenarios. The motion direction of π^+ in laboratory is depicted by the thick (blue) arrow. The outgoing directions of μ^+ and the associated neutrino in c.m. of π^+ are represented by the long arrows (black), the spin alignments are denoted by the thin arrows (red).

the strong absorption of the later, and the charge ratio $R(\mu^+/\mu^-) > 1$ [14], net negative polarization of the cosmic-ray muons is expected and it can be regarded as an indirect signature of PV in weak interactions.

The polarization of cosmic-ray muon, carried by forward–backward asymmetry of the decay, can be measured using the delay-coincidence method. Namely when a muon is stopped and identified in one of the scintillators, which is called absorber here, the decay e^- and e^+ are expected to be recorded in the scintillator below or above the absorber based on the event-by-event logics. The polarization can be deduced by the up–down (equivalently forward–backward) counting asymmetry α_e of the decay e^- and e^+. However, it should be pointed out that in such measurements the efficiency with which the decay e^- and e^+ are recorded in the detectors located at the two sides (up and down) of the absorber with finite thickness can be very different due to the strong multi scattering effect of e^- and e^+. Depending on the thickness of the absorber, the deviation of α_e is usually larger than the value of α_e. Thus careful investigation is required in order to confirm a non-zero asymmetry α_e.

The stop-and-decay scheme is applied to measure the decay of cosmic-ray muons. The apparatus consists of six pieces of scintillator detectors installed in a vertical row as shown in figure 2(a). Each scintillator has the dimension of $25 \times 25 \times 5$ cm^3. The scintillator is covered by aluminum foil as reflection material and Teflon tape as reinforce, then packed by black tape for light-tight shielding. The well-packed scintillator is placed in a box. The top and bottom faces of the boxes are made of ABS plastic sheets with thickness of 2 mm, while the side faces is made of aluminum frame. The scintillator array is installed on an aluminum frame and the distance between each neighboring detectors is 20 cm. The signals are all readout by photo multiplier tube (PMT) of the type CR161 from HAMAMATSU. The diameter of the PMT (sensitive window) is about 34 mm and it is coupled to the scintillator directly with optical grease. The shape of the amplified analog signals are sampled and digitized by the waveform digitizer V1720 (CAEN, Italy) and transferred to data acquisition computer via light fiber.

Two types of events can be recorded. One is the penetrating muon event, marked as I in figure 2(b) in which the muon penetrates the six scintillators. It requires that all scintillators are fired within a given time gate. These events can be used to calibrate the energy response of the scintillator. The other is the stop-and-decay muon event, marked as II in figure 2(b),

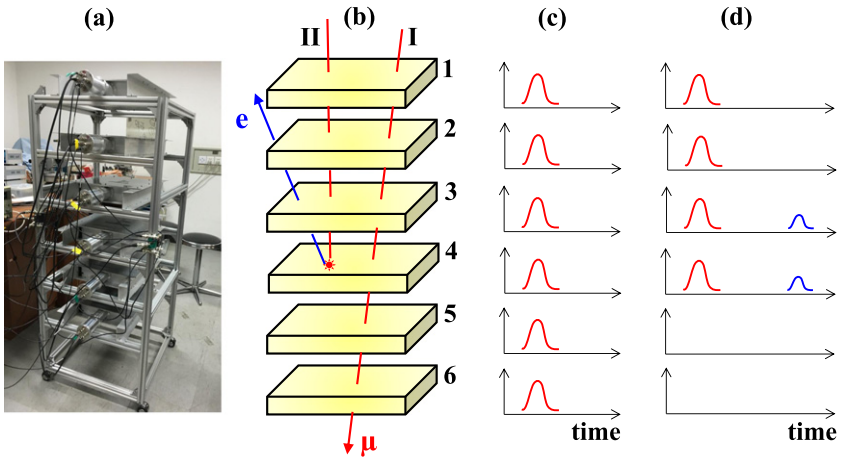

Figure 2. The experimental setup and the principle of the measurement. Panel (a) presents a picture of the setup and (b) presents a schematic view with the muon paths in two types of events. Panel (c) and (d) show the coincidence scheme of the penetrating muon events (I) and the stopped muon events (II), respectively.

in which a cosmic-ray muon is stopped in the ith ($i = 2, 3, 4, 5$) scintillator, and the decay e^- and e^+ can be detected by the scintillator above or below the last scintillator absorbing the incident muon. The trigger condition of the stop-and-decay event requires firing signals from the scintillators above the absorber and a veto given by the scintillator below within a short time gate, expressed by $12\bar{3} + 23\bar{4} + 34\bar{5} + 45\bar{6}$ where $+$ means logical OR and the short bar above a number represents the veto given by the corresponding scintillator. If a stop-and-decay event is identified, the signal of the decay e^- and e^+ is then searched in both scintillators neighboring to the absorber within a given coincidence window. According to which scintillator detects the decay e^- and e^+, the stop-and-decay events are further classified as up-events and down-events, corresponding to the events with the decay e^- and e^+ flying upward (opposite to the incident muon direction) and downward (along the incident muon direction), respectively. The coincidence time sequences for event I and II are schematically displayed in figures 2(c) and (d), respectively. Clearly, the stopped muon in (d) can be identified because one of the trigger conditions $34\bar{5}$ is satisfied.

In the stopped muon events, one can define the up–down asymmetry of the number of decay e^- and e^+ α_e as

$$\alpha_e = \frac{N_u - N_d}{N_u + N_d} \tag{1}$$

where N_u and N_d denotes the number of the up-events and down-events, which are recorded in the scintillator above or below the absorber, respectively. It can be an indicator of the polarization of the decay of muon.

3. Monte-Carlo simulations

Before physical data taking, we conducted full simulations to gain the knowledge of the detector response using Geant 4 packages [13]. In the simulations, both the body of the scintillator

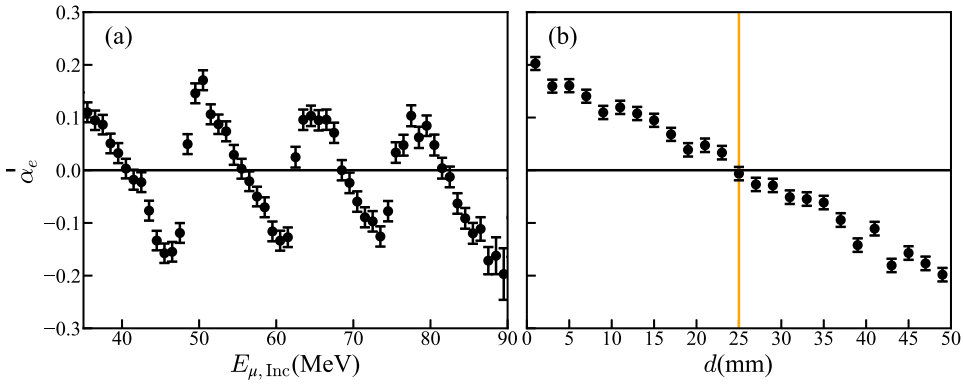

Figure 3. Geant 4 simulation of the detection of up–down asymmetry α_e. (a) The α_e as a function of the kinetic energy $E_{\mu,\mathrm{Inc}}$ of the incident μ^-. The four periods correspond to the scintillator 2 to 5, respectively. (b) The α_e as a function of the stopping depth d in a single scintillator.

assigned as sensitive volume and the covering materials are constructed. The ionization process, the decay of muons and the bremstrahlung process of electrons are all registered in the physical process list. The original muon energy is distributed uniformly from 0 to 100 MeV to cover the whole stopping depth of all the scintillators. The muons above this energy range will penetrate the devices and the decay cannot be detected. And thus, the results are relevant to the muons in this range. The polarization rate of $\alpha_e = 0$ is used as initial condition. The energy loss of the flying muons, the timing and energy deposit of the stopped muon and the timing and the energy loss of the decay e^- and e^+ are recorded in the sensitive detectors. The data generated in the simulations are analyzed using the same procedure as that in the experiment.

Figure 3(a) presents the results of the up–down asymmetry α_e extracted from the simulated events as a function of the kinetic energy of the incident muon $E_{\mu,\mathrm{Inc}}$. In the simulation we take μ^- as the example. Very interestingly, despite of the symmetrical structure of the array and the uniformity of scintillator material, the up–down asymmetry calculated by ansatz (1) exhibits a pattern oscillating around the initial value $\alpha_e = 0$ as a function of incident energy $E_{\mu,\mathrm{Inc}}$. The four periods on the plot correspond to the four sets of scintillator from No. 2 to 5. Apparently the variation of α_e is approximately ± 0.2, which is larger than the effect supposed to be observed.

The main reason of the large oscillation of α_e is due to the variation of the detection efficiency of the decay electron, which experiences large multiple scattering in the thick material [14]. For larger stopping depth of the muon, the decay electron flying upwards (downwards) passes thicker (thinner) materials causing more (less) loss in detection efficiency. Thus the α_e becomes smaller and vice versa. This effect can be equally observed in the correlation between α_e and the stopping depth d of the incident muon in a single scintillator, as shown in figure 3(b). Again because the detecting efficiency of the decay electrons is strongly correlated to the thickness of the scintillator it needs to pass though regardless the flying direction, the up–down asymmetry α_e decreases linearly with the stopping depth. When the muon stops near the upper surface, the electron emitted upward is more likely detected and α_e is calculated apparently high. Only when the muon stopped in the middle of the target absorber, as indicated by the vertical line, α_e can faithfully represent the polarization degree of the decay of the stopped muon.

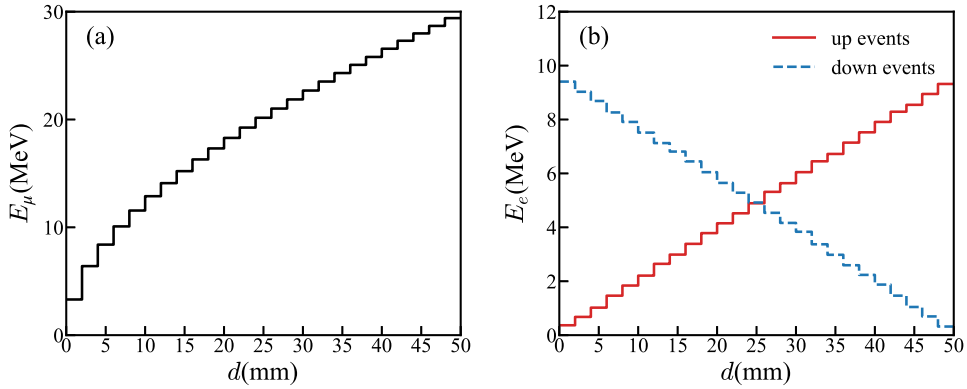

Figure 4. (a) The correlation between the stopping depth d and the energy deposit E_μ of the stopped μ^-. (b) The correlation between the energy loss of the decay electron and the stopping depth of μ^- for the up- (red) and down-events (blue), respectively.

It is inferred by the pattern in figure 3 that systematic uncertainty exists if one derive the up–down asymmetry using ansatz (1) only from the integrated counts, unless the muons are stopped uniformly along the depth in the scintillator by assumption. Otherwise in order to circumvent the unknown systematic uncertainty, it is required to identify the events where the muons are stopped in the vicinity of the middle point of the absorbing scintillator.

The energy deposit of the stopped μ^- or the energy loss of the decay electron in the absorber scintillator can be used as a rough measure of the stopping depth of the μ^-, even though the emission direction of the decay electron varies. Figure 4 shows the correlation between d and the energy deposit of muon E_μ (a) and the energy loss of the decay electron E_e (b) in the absorber scintillator, respectively. In panel (b) the events are sorted in two groups, i.e., the up-events (red) and the down-events (blue), respectively. It is shown that both E_μ and E_e are approximately linear to the stopping depth d of the muon. Reasonably, at the middle point of d, the average E_e of up events and down events are equal because the perpendicular thickness of the scintillator material is the same for the electrons flying upwards and downwards. This character will be used in the experimental data analysis to determine the position of the middle point, see next.

Combining all the correlations, we come up with a new scheme of data analysis, i.e., E_μ is used to characterize d indirectly. Figure 5(a) depicts the correlation between α_e and E_μ under different conditions. Surveying the ideal data (blue symbols) of the energy deposit E_μ (as will be detailed below), a nearly linear falling pattern is evident similar with the α_e–d correlation in figure 3(b).

However, both the experimental threshold of the signal and the finite energy resolution will weaken the α_e–E_μ correlation. If there is an experimental threshold cut imposed on E_μ and particularly on E_e, the decay events occurred at both surfaces of the absorber with the electron flying away will be undetected largely because E_e can be too small to pass the threshold. As a result, the α_e will be much below (above) the ideal correlation line at the low (high) end of E_μ, as indicated by the open circle symbols in figure 5(a) where a threshold of 1 MeV is applied. In addition, it is found that a finite energy resolution reduces the α_e–E_μ slope and enhances the deviation at high energy end of E_μ, causing the up-bending to appear earlier (red triangle symbols). Thus, in real experiment, where the energy signal is degraded by the intrinsic energy resolution and the non-uniformity of response against the variation of the incident position, the data range contains faithfully the α_e–E_μ correlation will be much narrower, for instance, the

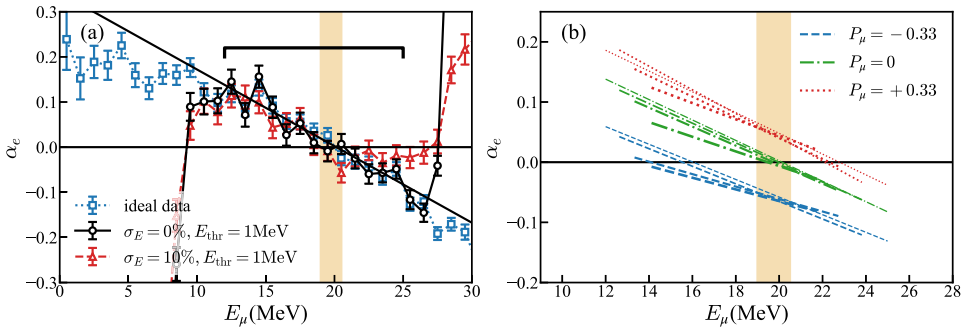

Figure 5. (a) The correlation between the extracted up–down asymmetry $\alpha_{\rm e}$ and the energy deposit of the stopped muon E_{μ} in the absorber scintillator under different condition, i.e., without (blue square) and with energy threshold cut (open circle) plus energy smearing (red triangle). The cap indicates the good rang for fitting. (b) The $\alpha_{\rm e}$–E_{μ} with different energy smearing 0, 5%, 10% and 15% in the absorber, indicated by the increase of the thickness of the dashed lines in each group. Three initial polarizations $P_{\mu} = -0.33$ (blue), 0 (green) and 0.33 (red) are assumed, respectively. The vertical shadow bands in (a) and (b) indicate the energy loss of the muon stopped at the middle of the absorber.

range from 12 to 25 MeV can be used to conduct the linear fit, as indicated by the cap in figure 5(a).

Figure 5(b) presents further the effect of variation of the energy resolution on the $\alpha_{\rm e}$–E_{μ} correlation. Here we set the threshold at 0 to view the effect of energy resolution clearly. Simulations have been performed for 3 groups of muon events with the polarization rate of $P_{\mu} = -0.33$, 0 and 0.33, represented by blue, green and red dashed lines, respectively. The absolute value of 0.33 is taken according to the reported experimental results [14]. It is shown that by increasingly smearing the energy resolution from 0 to 15%, as indicated by the increasing thickness of the dashed lines, the slope of the $\alpha_{\rm e}$–E_{μ} correlation decreases. Although the correlation is weakened, the pattern still survives. At the mean stopped depth as indicated by the vertical shadow band, the up–down asymmetry in the case of $P_{\mu} = -0.33$ is about 0.05, which is supposed to be dependent on the setup parameters such as the opening angle and the absorber thickness etc.

4. Data analysis and results

Totally 50 086 stop-and-decay events were recorded in the 2 months data taking with an event rate of 1.5 min^{-1} approximately. The long-time data taking was to ensure the sufficient statistics in each bin of E_{μ}. Besides, 67 684 (36 478) penetrating events were collected with a rate of 5 events per second, which is much higher than the stop-and-decay rate, before (after) the 2 months data taking of the stop-and-decay events to calibrate the signal magnitude of the scintillators. The data analysis was done by using the ROOT packages [15]. The calibration procedure, the derivation of the life time and the extraction of the polarization rate of the cosmic-ray muons will be described in this section.

4.1. Energy and timing calibration

It is reasonable to assume that the energy loss distribution of the cosmic-ray muons penetrating all scintillators are the same, since the material and the geometric structure are identical for

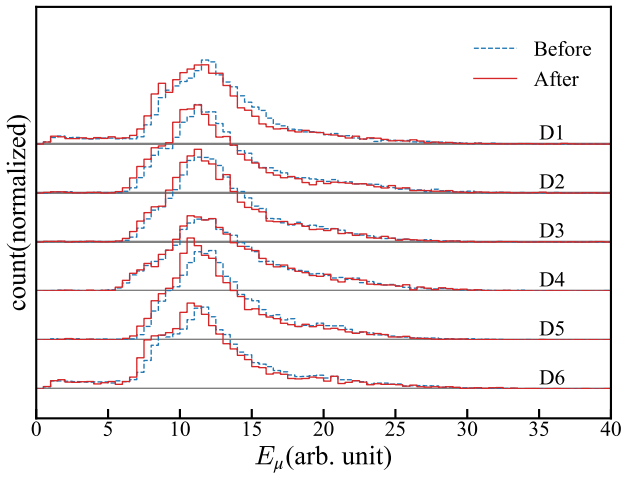

Figure 6. The energy loss spectra of the penetrating muons in the scintillators before (blue dashed) and after (red solid) the data taking of the stop-and-decay muon events. The energy response of the scintillator was not calibrated and arbitrary unit was used.

all the untis. Considering that the amplification of each individual PMT can be slightly different, we tuned finely the high voltage of each PMT to maintain the uniformity of the signal amplitudes of the energy outputs. Figure 6 presents the energy loss distributions of the penetrating muons in the scintillators from 1 to 6 before (blue dashed) and after (red) the data acquisition of the stop-and-decay events. Because the response of the scintillator is not necessarily linear and the light output depends on the incident position, a precise energy calibration is not valid in our measurement and arbitrary unit is assumed. Nevertheless, it is verified that the variation of the peak positions of the six detectors has been controlled within 5%, which is acceptable in our experiment since the level of the variation is much better than the intrinsic energy resolution of the plastic scintillators. Besides, the peak positions of the spectra are not changed before and after the data acquisition, ensuring the stability of the responses of the PMTs.

We also checked the standard deviation distribution of the timing in six scintillators for the penetrating events. The sampling period of the V1720 waveform digitizer is 4 ns, corresponding to a sampling frequency of 250 MHz. Assuming that the high energy muons fly with the speed of light, it takes about 3 ns to pass through the whole apparatus. The distributions demonstrate consistently that most of the events have a standard deviation less than 4 ns. Thus, we use the 3σ limit as our time gate for coincidence between different scintillators.

4.2. Mean life time of muons

Before extracting the polarization rate of the decay muons including both μ^- and μ^+ in experiment from the stop-and-decay events, we first derived the mean life time of the decay muons. The distribution of the decay time, defined by the difference between the time of the decay e^- and e^+ and the arrival time of the incident muon, is displayed with logarithmic scale in figure 7. The red, blue and black histograms represent the up events, down events and the total events respectively. In the range below approximately $t \leqslant 15$ μs, the feature of the exponential decay is evident. In the time range with $t > 15$ μs, however, a flat distribution is shown in accordance with a constant background contribution, as shown by the dashed line. Thus, the

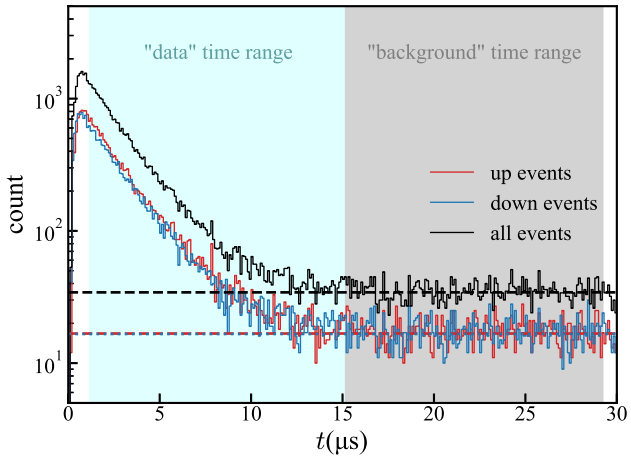

Figure 7. The life time spectra of the decay muons. The red, blue and black histograms represent the up events, down events and the total events respectively. The time window 15.2–29.2 μs is used for the background estimation.

whole distribution is fitted using

$$N = N_0 \left[\exp\left(-t/\tau\right) + b\right] \tag{2}$$

where τ is the life time of muon and the constant b reflects the background level triggered by random coincidence. Here N_0, τ and b are all free parameters in the fit. In the data analysis, the events in the decay time window 1.2–15.2 μs were accumulated for stop-and-decay analysis, subtracting the contamination of the background which was obtained in 15.2–29.2 μs.

The mean life time extracted from the fit is 2109 ± 18, 2102 ± 25 and 2105 ± 26 ns for the total events, the up-events and the down-events, respectively, where the standard deviation is presented. Interestingly, although the values are identical for all the three groups within uncertainty, the life time values are marginally smaller than the nominated value of muons 2197.03(4) ns. The difference can be interpreted by the capture of the μ^- by the target nuclei. Since μ^- is the second generation of lepton in analog with electron, it can be probably captured by the nuclei once it is stopped in the material. The capture will change the decay time spectrum and reduce the life time extracted from the exponential fit [16]. It has been observed that the absorption depends sensitively on the atomic number of the target material. For the plastic scintillator made of H, C, and O elements, causing 0.13%, 7% and 17.5% reduction of the life time of pure μ^- respectively [16], the slight decrease of the life time in our experiment is reasonable.

4.3. E_μ spectrum and α_e–E_μ correlation

Figure 8(a) presents the energy spectra of the stopped muons recorded in the decay time window of 1.2–15.2 μs in the stopping scintillators before subtracting the background. In total, 12 266, 12 186, 13 098 and 12 536 events are selected within the decay time window in the four scintillators from 2 to 5, respectively. They are summed up in the plot in figure 8(a) for the up- and down-events, respectively. It is shown that both spectra exhibit a sudden drop on the high energy side corresponding to the maximum energy loss. On the slow rising part, however, there is a wide bump near $E_\mu = 10$–15 (arb. unit) similar with the energy loss of the penetrating

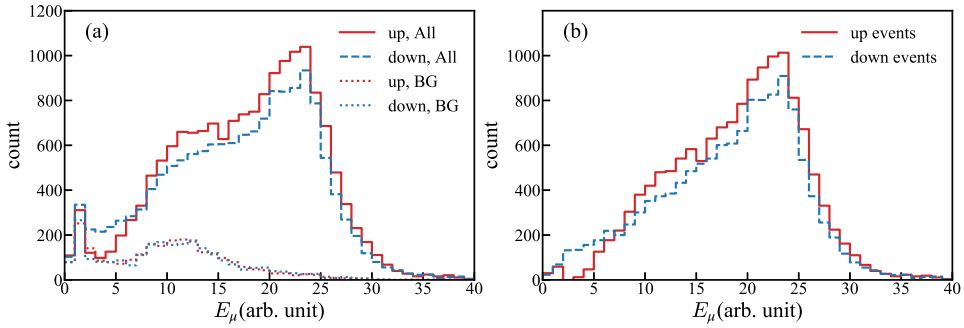

Figure 8. The energy spectra of the stopped muons before (a) and after (b) subtracting the background for the up-events (red) and down-events (blue), respectively.

muon. The energy spectra of the muons in the time window of 15.2–29.2 μs are represented by the dotted curves, which can be regarded as the background recorded by random coincidence since this time is much longer than the lifetime of muon. Interestingly, the peak of the background distribution is in accordance with energy loss distribution of the penetrating muon events in figure 6. Then, as shown in figure 8(b), the net energy deposit spectra of the stopped muon are obtained by subtracting the background from the total energy spectra in panel (a). Two features can be viewed if one inspects the net energy spectra carefully. First, the rising slope of the energy spectra is now approximately uniform after the background subtraction. Second, in the whole range of the main peak, the yields of the up-events is constantly larger than the down-events (with an exception in the very low energy part $E < 5$ arb. unit, where a lot of events are undetected because of the threshold), indicating an averagely negative polarization rate of the cosmic-ray muons as predicted in the existing literature. Summing the whole range, one can derive an integrated polarization rate of $\alpha_{\mathrm{e,Int}} = 0.058 \pm 0.006$ (only standard statistical uncertainty) without taking into account its variation as E_μ.

As pointed out in the simulation, one must inspect the correlation of α_e and E_μ representing approximately the stopping depth. Figure 9 presents the extracted α_e as a function of E_μ. The bin width is chosen as 1 (arb. unit). The error bars shown in the figure represent only the statistical uncertainty. It is found that despite of the large uncertainty, in the range of the main peak, the correlation between α_e and E_μ is exhibited. Because of the experimental threshold and the low energy resolution of the detector, the correlation is largely suppressed in comparison with the simulation using the calculated energy deposits. Nevertheless, all the points are located beyond $\alpha_\mathrm{e} = 0$ in agreement with the integrated results, and the decreasing trend supports the pattern found in the simulation. It is noticed in figure 9 that the data points with $E_\mu \leqslant 10$ and $E_\mu \geqslant 20$ (arb. unit), represented by the gray points, are distorted due to the threshold and the energy smearing effect elucidated in figure 5(a) and in figure 10 (see next), thus in order to quantify the decreasing trend, only the data points (black points) in the channels of $E_\mu = 11$–19 (arb. unit), where the energy spectra are not distorted, are fitted using a linear function

$$\alpha_\mathrm{e} = kE_\mu + b \tag{3}$$

The fit yields a straight line with $k \pm \sigma_k = -8.6 \pm 5.7 \times 10^{-3}$ and $b \pm \sigma_b = 0.22 \pm 0.09$, as shown by the solid line in the figure. We have approximately a 1.5σ confidence that the falling correlation pattern between the stopping depth d and α_e exists.

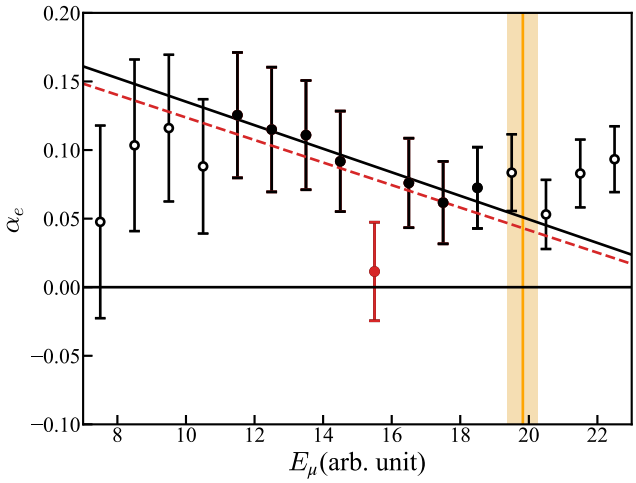

Figure 9. The graph of E_μ–α_e pattern and the fitting results. The red dashed line is the fitting result of all points between $E_\mu = 11$–19 (arb. unit), while the solid black line is the fitting result excluding the outlier point (red solid circle) at $E_\mu = 15$ (arb. unit). The cyan vertical band indicates the crossing point of E_μ–E_e pattern, see figure 10.

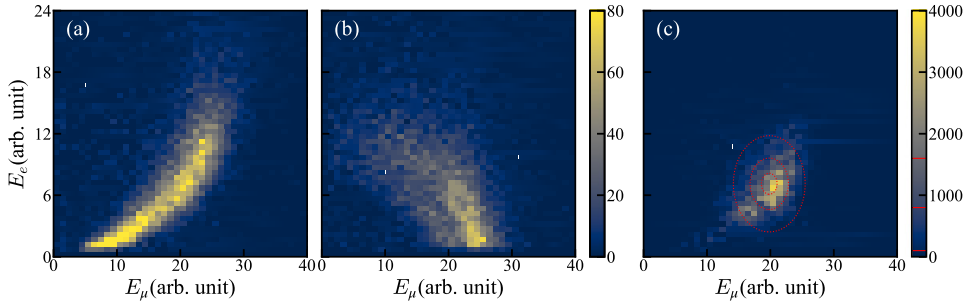

Figure 10. E_μ–E_e correlation of up- (a) and down-events (b) and their product intensity histogram (c), the two dimensional Gaussian fit result of the product histogram is plotted by the contour curves (red dashed) in (c).

4.4. E_μ–E_e correlation

Now, we can further extract the up–down asymmetry of the cosmic-ray muons from the α_e–E_μ correlation. The key point is to locate the middle depth of the scintillator. Figures 10(a) and (b) are the scattering plot of E_μ and E_e for the up-events and down-events, respectively. Although the energies of both muons and decay e^- and e^+ distribute broadly because of the limited energy resolution and the scattered direction, considering the nonlinear response of the scintillator, the monotonous E_e–E_μ correlation shown in panels (a) and (b) is qualitatively consistent with the picture unraveled by the simulation. Nevertheless, it is shown in both panels that the events near $E_e = 0$ are cut out, leading to the distortion of the α_e–E_μ correlation at both the left and the right ends of E_μ in figure 9.

Now one can locate the mean stopping depth from the two histograms of figures 10(a) and (b) as following. Considering the monotonous feature of E_e–E_μ correlation for both groups

of events, we multiply the intensity of the two histograms of (a) and (b) bin-by-bin and plot the product intensity histogram in figure 10(c). It is shown that the point corresponding to the mean stopping depth manifests itself by a peak with the highest intensity. A two dimensional Gaussian fit is conducted to the product histogram, as presented by the contour curves in panel (c), showing the peak located at $E_\mu \pm \sigma_{E_\mu} = 19.8 \pm 0.1$. Using the fitting results from equation (3), one writes

$$\alpha_{\mathrm{e}} \pm \sigma_{\alpha_{\mathrm{e}}} = 0.051 \pm 0.027 \tag{4}$$

The result suggests that at about 90% confidence level (2σ), the up–down asymmetry of the decay of cosmic-ray muon is observed. Within the uncertainty limit, it is indeed consistent with the integration result of $\alpha_{\mathrm{e,Int}} = 0.058 \pm 0.006$. In order to improve the precision of the experiment, detectors with better energy resolution and smaller opening angle are demanded. In addition, more statistics are preferred to reduce the statistical uncertainty in each E_μ bin.

Finally, it should be pointed out that the measurement of the muon spin asymmetry would be easier and more accurate if a magnetic field can be provided covering the space where the muons (usually charge-identified) are stopped, as done in the original accelerator-based experiment of muon spin rotation [5].

5. Conclusion

In conclusion, in the student physics laboratory of the Department of Physics, Tsinghua University, a scintillator detector array has been set up to measure the decay of cosmic-ray muons in a stop-and-decay scheme. It has been observed that due to the multiple scattering of the electrons or positrons, the up–down asymmetry of the decay of the incident muon exhibits a correlation with the stopping depth, which can be represented approximately by the energy deposit of the muon in the absorber detector. The amplitude of the correlation pattern is comparable with the initial asymmetry of the decay of cosmic-ray muon and may bring systematic uncertainty to the direct measurement of the up–down asymmetry. At nearly 90% confidence level, the experimental result with $\alpha_{\mathrm{e}} \pm \sigma_{\alpha_{\mathrm{e}}} = 0.051 \pm 0.027$ confirms the observation of the up–down asymmetry of the decay of cosmic-ray muon. The experiment can be constructed with reasonable cost in student laboratory of universities and provides a pedagogic view of the evidence of the PV of weak interaction without offering a magnetic system which is usually expensive. This experiment is on the level of student research training program, where the participants receive training on both detector hardware operation as well as the development of data analysis software particularly on histograming, which is essential to build the concept of the statistical data analysis.

Acknowledgments

Two groups of undergraduate students in the third year have dedicated in the experiment successively. The group of JX, XS and ZY set up the experiment and obtained the integrated up–down asymmetry. The group of JX, AC and TC found and confirmed the correlation pattern between the up–down asymmetry and the stopped depth. JX did the data analysis and made all the figures. AC did the G4 simulations and ZY designed the original version of the readout electronics. HY and YW were the teaching assistants in the course helping the students with laboratory training. YC and ZZ helped with the organization of the experiment. ZX led the

experimental project and wrote the manuscript. The work is supported by Tsinghua Student's Laboratory Innovation Program, the Platform of the Laboratory Physics Teaching Center of THU and Tsinghua Xuetang Talents Program.

ORCID iDs

Yijie Wang https://orcid.org/0000-0003-2692-8985
Zhigang Xiao https://orcid.org/0000-0001-9534-5981

References

[1] Lee T D and Yang C N 1965 *Phys. Rev.* **104** 254
[2] Wu C S, Ambler E, Hayward R W, Hoppes D D and Hudson R P 1957 *Phys. Rev.* **105** 1413
[3] Frauenfelder H, Bobone R, von Goeler E, Levine N, Lewis H R, Peacock R N, Rossi A and De Pasquali G 1957 *Phys. Rev.* **106** 386
[4] Goldhaber M, Grodzins L and Sunyar A W 1958 *Phys. Rev.* **109** 1015
[5] Garwin R L, Lederman L M and Weinrich M 1957 *Phys. Rev.* **105** 1415
[6] Griffiths D 1987 *Introduction to Elementary Particles* (New York: Wiley)
[7] Blundell S J 1999 *Contemp. Phys.* **40** 175
[8] Nagamine K *et al* 2014 *J. Phys.: Conf. Ser.* **551** 012064
[9] Fujimaki T *et al* 2017 *PoS* PoS(ICRC2017)221
[10] Pohl R *et al* 2010 *Nature* **466** 213
[11] Mühry H and Ritter P 2002 *Phys. Teach.* **40** 294
[12] Bosnar D, Matić Z, Friščić I, Žugec P and Janči H 2018 *Eur. J. Phys.* **39** 045801
[13] Agostinelli S *et al* 2003 *Nucl. Instrum. Methods* A **506** 250
[14] Turner R, Ankenbrandt C M and Larsen R C 1971 *Phys. Rev.* D **4** 17
[15] Brun R and Rademakers F 1997 *Nucl. Instrum. Methods Phys. Res.* A **389** 81
[16] Suzuki T, Measday D F and Roalsvig J P 1987 *Phys. Rev.* C **35** 2212